Growth and neurite stimulating effects of the neonicotinoid pesticide clothianidin on human neuroblastoma SH-SY5Y cells

Tetsushi Hirano[a,*], Satsuki Minagawa[a], Yukihiro Furusawa[b], Tatsuya Yunoki[c], Yoshinori Ikenaka[d,e], Toshifumi Yokoyama[f], Nobuhiko Hoshi[f], Yoshiaki Tabuchi[a]

[a]*Life Science Research Center, University of Toyama, Toyama, Toyama, Japan*
[b]*Department of Liberal Arts and Sciences, Toyama Prefectural University, Toyama, Toyama, Japan*
[c]*Department of Ophthalmology, Graduate School of Medicine and Pharmaceutical Sciences, University of Toyama, Toyama, Toyama, Japan*
[d]*Laboratory of Toxicology, Department of Environmental Veterinary Sciences, Faculty of Veterinary Medicine, Hokkaido University, Sapporo, Hokkaido, Japan*
[e]*Water Research Group, Unit for Environmental Sciences and Management, North-West University, Potchefstroom, South Africa*
[f]*Department of Animal Science, Graduate School of Agricultural Science, Kobe University, Kobe, Hyogo, Japan*

Abbreviations: nAChR, nicotinic acetylcholine receptor; CTD, clothianidin; ACE, acetamiprid; IMI, imidacloprid; NOAEL, no observed adverse effect level; DHβE, dihydro-β-erythroidine; MEC, Mecamylamine; MLA, methyllycaconitin

*Corresponding author at: Life Science Research Center, University of Toyama, 2630 Sugitani, Toyama 930-0194, Japan.
E-mail address: thirano@cts.u-toyama.ac.jp (T. Hirano).

ABSTRACT

Neonicotinoids are one of most widely used pesticides targeting nicotinic acetylcholine receptors (nAChRs) of insects. Recent epidemiological evidence revealed increasing amounts of neonicotinoids detected in human samples, raising the critical question of whether neonicotinoids affect human health. We investigated the effects of a neonicotinoid pesticide clothianidin (CTD) on human neuroblastoma SH-SY5Y cells as *in vitro* models of human neuronal cells. Cellular and functional effects of micromolar doses of CTD were evaluated by changes in cell growth, intracellular signaling activities and gene expression profiles. We examined further the effects of CTD on neuronal differentiation by measuring neurite outgrowth. Exposure to CTD (1–100 μM) significantly increased the number of cells within 24 hours of culture. The nAChRs antagonists, mecamylamine and SR16584, inhibited this effect, suggesting human α3β4 nAChRs could be targets of neonicotinoids. We observed a transient intracellular calcium influx and increased phosphorylation of extracellular signal-regulated kinase 1/2 shortly after exposure to CTD. Transcriptome analysis revealed that CTD down-regulated genes involved in neuronal function (e.g., formation of filopodia and calcium ion influx) and morphology (e.g., axon guidance signaling and cytoskeleton signaling); these changes were reflected by a finding of increased neurite length during neuronal differentiation. These findings provide novel insight into the potential risks of neonicotinoids to the human nervous system.

Keywords: Neonicotinoid; Pesticide; Clothianidin; Neuroblastoma cell; Nicotinic acetylcholine receptor; Intracellular signaling.

1. Introduction

Neonicotinoids are the most recent and widely used class of pesticides to control harmful insects in the world. With expanding use of the pesticides in farming, multiple neonicotinoids are present in most vegetables, fruits and crops at parts-per-billion concentrations (Chen et al., 2014; Ikenaka et al., 2018). In fact, neonicotinoids were detected in urine samples from most adults and children (Ueyama et al., 2015; Ikenaka et al., 2019) and the urinary concentration of total neonicotinoids in Japanese children has been reported to be in the hundreds-level nanomolar (Osaka et al., 2016). Neonicotinoids act as nicotinic acetylcholine receptor (nAChR) agonists with as much as hundreds fold greater affinity for insect nAChRs than for mammalian receptors (Tomizawa and Casida, 2005); however, adverse effects on physiological function of non-target vertebrates have been reported over the last decade (Hoshi et al., 2014; Gibbons et al., 2015; Wang et al., 2018). *In vitro* studies have shown that potency and specificity for mammalian nAChRs are critically different among types of neonicotinoids (Casida, 2018). In particular, Kimura-Kuroda et al. (2012) firstly showed that acetamiprid (ACE) and imidacloprid (IMI), earlier chloropyridylmethyl neonicotinoids, caused neural excitation in cerebellar cells from neonatal rats mediated by nAChRs. These ligand-gated ion channel receptors play a variety of roles in multiple areas of the mammalian brain, including not only cholinergic transmission but also neural excitability and synaptic plasticity (Gotti, et al., 2006; Dani and Bertrand, 2007). Thus, there is increasing concern about the risks of neonicotinoids on the central nervous system in mammals.

Recent rodent studies indicated that a variety of neonicotinoids have neurobehavioral effects on mammals depending on the timing of exposure. We previously reported that at or below the no observed adverse effect level (NOAEL) of a later-developed chlorothiazolylmethyl neonicotinoid, clothianidin (CTD) resulted in anxiety-like behavior

and human-audible vocalization in a novel environment in mature mice (Hirano et al., 2015, 2018). Gestational and postnatal exposure of an early-type of neonicotinoid, ACE induced behavioral changes including increasing of sexual and attacking behavior in mature offspring (Sano et al., 2016), whereas IMI decreased social aggression behavior (Burke et al., 2018). In addition, pre- and postnatal exposure to the latest neonicotinoid, dinotefuran increased the number of dopaminergic and serotonergic neurons in the midbrain of mature mice (Takada et al., 2018; Yoneda et al., 2018). Although no common effects associated with the developmental neurotoxicity were observed among neonicotinoids (Sheets et al., 2016), differentiative neurons in the mammalian developing brain could be a potential target of neonicotinoids.

It has been noted that the amount and detection rate of neonicotinoids in human-derived samples are increasing gradually every year (Ueyama et al., 2015). Although human population studies reported that environmental exposure to neonicotinoids associated with adverse neurological outcomes such as memory loss and finger tremor, experimental studies of risks of neonicotinoids in humans are still far from sufficient (Cimino et al., 2017). Most toxicological data for evaluating the effects of neonicotinoids were obtained from *in vitro* and *in vivo* studies using rats and mice as animal models; however, there are evolutionary differences in the amino acid sequence of nAChRs subunits between rodents and human (Tsunoyama and Gojobori, 1998; Stokes et al., 2015). Therefore, the intensity and dose responses of nAChRs to nicotinic agonists can be different across species (Papke and Porter Papke, 2002; Anderson et al., 2008), suggesting that there is some uncertainty to predict the risk of modulating the function of human-type nAChRs from other species.

In the present study, we focused on CTD which has been banned in the European Union since 2013; however, it became a first-line pesticide for farming in many countries.

Intraperitoneally-administered CTD was immediately absorbed and reached throughout the body in mice including the brain at least a few hours (Ford and Casida, 2006). The aim of the present study is to provide novel experimental data for assessing whether CTD could affect human nervous system structure or function, using a human neuroblastoma cell line SH-SY5Y cells known to have high expression levels of neuronal types of nAChRs that contain α3, α7, β2, and β4 subunits (Lukas et al., 1993; Groot Kormelink and Luyten, 1997; Kovalevich and Langford, 2013) instead of animal models. We investigated the potential effects of CTD on cell growth and development, and examined mechanisms of action focusing on intracellular signaling and gene expression profiles.

2. Materials and methods

2.1. Cell culture and chemical treatments

Human neuroblastoma SH-SY5Y cells (ECACC, No. 94030304) were maintained in Dulbecco's Modified Eagle's Medium (DMEM) with 10% fetal bovine serum (FBS), 100 U/ml penicillin and 100 μg/ml streptomycin at 37°C in humidified air with 5% CO_2. Clothianidin (CTD; purity > 99.8%; Sigma-Aldrich, St. Louis, MO, USA), dihydro-β-erythroidine hydrobromide (DHβE; Tocris Bioscience, Ellisville, MO, USA) and SR 16584 (Cayman Chemical Co., Ann Arbor, MI, USA) were dissolved in dimethyl sulfoxide (DMSO). Mecamylamine hydrochloride (MEC; Sigma-Aldrich) and methyllycaconitine citrate (MLA; Cayman Chemical Co.) were dissolved in sterilized water. In all experiments, cells treated with corresponding vehicle (0.1% v/v) were used as a control.

2.2. Cell growth assay

For cell counting assays, cells were subcultured in 12-well plates at a seeding density 5.0 ×

10^4 cells/mL with 1 mL of the culture medium for 24 h, and then exposed to 1 or 100 µM CTD with reference to previous *in vitro* studies (Kimura-Kuroda et al., 2012; Christen et al., 2017). After washing once with phosphate-buffered saline (PBS) and subsequent trypsinization, the number of cells was counted using a hematocytometer on Day 1 and 2. For antagonist assays, cells were exposed to nAChR antagonists concomitantly with 100 µM CTD and counted on Day 1. For microplate assays, cells were plated into 96-well plates at a seeding density 5.0×10^4 cells/mL with 100 µL of the culture medium for 24 h, and then exposed to various concentrations of CTD (1 nM to 100 µM) for 24 h. Cells were then incubated with 2-(2-methoxy-4-nitrophenyl)-3-(4-nitrophenyl)-5-(2,4-disulfophenyl)-2H-tetrazolium (WST-8; Dojindo Laboratories, Kumamoto, Japan) solution for 3 h and the absorbance at 450 nm was measured by a BioRad 680 microplate reader (BioRad, Hercules, CA, USA).

2.3. Fluo-4 calcium flux assay

Changes in intracellular calcium concentration were measured with a fluo-4 kit (Dojindo Laboratories) according to the manufacturer's instructions. Briefly, semi-confluent cells in a 96-well microplate were loaded with 10 µM Fluo-4 AM in 100 µL of recording buffer [20 mM HEPES buffer containing 115 mM NaCl, 5.4 mM KCl, 0.8 mM $MgCl_2$, 1.8 mM $CaCl_2$, 13.8 mM glucose] and 0.02% Pluronic F-127 for 60 min at 37°C. Cells were washed with PBS, and then 90 µL of the recording buffer was added. After measuring baseline fluorescence for 1 min, test compounds dissolved in the recording buffer (10 µL) were added and changes in fluorescence (excitation 488 nm; emission 530 nm) were kinetically measured by a microplate reader (SpectraMax i3, Molecular Devices, Sunnyvale, CA, USA) for 2 min.

2.4. Western blotting

After 1 h of CTD treatment, semi-confluent cells were dissolved in ice-cold lysis buffer [50 mM Tris-HCl buffer (pH 8.0) containing 150 mM NaCl and 1% NP-40, supplemented with 1:1000 protease inhibitor cocktail and phosphatase inhibitor cocktail (Sigma-Aldrich)] and homogenized by an ultrasonic disruptor. Total protein concentrations of supernatant were determined using a Pierce BCA Protein Assay Kit (Pierce Biotechnology, Rockford, IL, USA), and then equal amounts of proteins from each sample were boiled in SDS sample buffer [in final concentrations of 60 mM Tris /HCl, 10% glycerol, 2% SDS, 5% mercaptoethanol, 0.025% bromophenol blue, pH 6.8] at 94°C for 5 min. Samples containing 10 μg of protein extract were separated in SDS-polyacrylamide gels and transferred to PVDF membranes. Membranes were blocked by PVDF Blocking Reagent for Can Get Signal (Toyobo Co., Ltd., Osaka, Japan) for 2 h at room temperature, and then incubated overnight at 4°C in Can Get Signal Immunoreaction Enhancer Solution 1 (Toyobo Co., Ltd.) with the rabbit anti-pERK antibody and mouse anti-ERK antibody (1:2000, #9101 and #9107, Cell Signaling Technology, Danvers, MA, USA). After washing 3 times with Tris-buffered saline containing 0.1% Tween 20, membranes were then incubated in Can Get Signal Immunoreaction Enhancer Solution 2 (Toyobo Co., Ltd.) with IRDye 680RD donkey anti-mouse IgG and IRDye 800CW goat anti-mouse IgG (1:2000; LI-COR Biosciences, Lincoln, NE, USA) for 2 h at room temperature. The Odyssey infrared imaging system (LI-COR Biosciences) was used to scan the infrared signal on membranes, and Image Studio 5.1 software (LI-COR Biosciences) was used to quantify the band intensity.

2.5. RNA isolation and Clariom S assay

After 24 h of 1 μM CTD treatment, total RNA was extracted from semi-confluent cells

using a NucleoSpin plus RNA isolation kit (Macherey-Nagel GmbH & Co., Düren, Germany) following the manufacturer's instructions. The quality of the RNA was analyzed using a Bioanalyzer 2100 and an RNA6000 Nano LabChip kit (Agilent Technologies, Inc., Santa Clara, CA, USA) and samples with RIN (RNA integrity number) values above 9.8 were considered acceptable. All RNA samples (500 ng) were amplified and labeled using the GeneChip WT PLUS Reagent Kit and hybridized with the Clariom S human arrays containing 21,448 probe sets (Affymetrix, Inc., Santa Clara, CA, USA). All microarrays were washed and stained on the GeneChip Fluidics Station 450 using the GeneChip Hybridization, Wash, and Stain Kit, and then scanned on the GeneChip Scanner 3000 (Affymetrix, Inc.). The raw intensity data were normalized and analyzed using GeneSpring GX 14.9 software (Agilent Technologies, Inc.). To examine the molecular functions of differentially expressed genes, data were analyzed using Ingenuity Pathways Analysis (IPA) tools (Ingenuity Systems, Mountain View, CA, USA). The microarray data (.CEL files) were deposited in a public database (Gene Expression Omnibus, accession number: GSE126103).

2.6. Quantitative reverse transcription PCR

RNA samples (1 μg) were reverse-transcribed to cDNA using a PrimeScript RT Master Mix (Takara Bio Inc., Shiga, Japan) following the manufacturer's instructions. Gene expression was quantified using SYBR Green Premix Ex Taq II (Takara Bio Inc.) with specific primers (Table 1) on an Mx3005P Real-Time QPCR System (Agilent Technologies, Inc.). Cycling conditions were as follows: An initial degeneration of 95°C for 30 sec, followed by 40 cycles of denaturing at 95°C for 5 sec, annealing at 55°C for 30 sec, and elongation at 72°C for 30 sec. Copy number of genes were calculated by standard curves and the relative gene expression levels are normalized by a housekeeping gene,

glyceraldehyde-3-phosphate dehydrogenase (GAPDH) using a MxPro software (version 4.10, Agilent Technologies, Inc.). All samples were measured in duplicate and the specificity of the PCR products was confirmed by melting curves.

2.7. Neurite outgrowth assay

Cells were plated on glass coverslips precoated with poly-L-lysine in 24-well plates at a seeding density of 5.0×10^4 cells/mL with 500 µL of the culture medium. For differentiation, cells were treated with FBS-free DMEM containing 10 µM all-trans retinoic acid (Sigma-Aldrich) for 3 days, followed by FBS-free DMEM containing 50 ng/mL of brain-derived neurotrophic factor (Alomone lab, Jerusalem, Israel) for 3 days with or without 1 or 100 µM CTD. After washing with PBS, cells were immediately fixed by 4% paraformaldehyde for 10 min and then permeabilized in 0.1% Triton-X in PBS for 10 min. Cells were blocked for 1 h with Blocking One Histo (Nacalai Tesque, Inc., Kyoto, Japan) and then incubated overnight at 4°C in Can Get Signal Immunoreaction Enhancer Solution A (Toyobo Co., Ltd.) with rabbit anti-MAP2 antibody (1:200, #4542, Cell Signaling Technology). After washing 3 times with PBS containing 0.1% Tween 20, cells were incubated for 2 h in Can Get Signal Immunoreaction Enhancer Solution B (Toyobo Co., Ltd.) with anti-rabbit donkey IgG (H&L) antibody conjugated to DyLight 549 (1:1000, #611-742-127, Rockland Immunochemicals, Inc., Gilbertsville, PA, USA). Cell nucleus was counterstained with 4’-6-diamidino-2- phenylindole (DAPI). The coverslips were mounted on microscope slides in ProLong Glass antifade mountant (Thermo Fisher Scientific, Waltham, MA, USA) and fluorescence images were acquired with a BX61/DP70 microscope (Olympus, Tokyo, Japan). Neurite length was measured in at least 100 cells in three randomly chosen fields using ImageJ software (version 1.51) with the NeuronJ plugin.

2.8. Statistical analyses

Results from at least three independent experiments are expressed as the mean ± standard deviation (SD). IBM SPSS statistics 23 software (IBM Co., Somers, NY, USA) was used to perform statistical analyses. The dose-response curve was fitted using the sigmoidal (4-parameter) equation with JMP13 Pro software (SAS Institute, Cary, NC, USA). The EC50 value was calculated by determining the concentration at which 50% of maximum activity was reached using the sigmoidal fit equation. One-way analysis of variance (ANOVA) followed by Dunnett's post-hoc test was used to analyze the effects of CTD. Two-way ANOVA followed by Tukey's post hoc test was used to analyze the interaction between CTD and nAChR antagonists. The Welch's *t* test was used to validate the microarray results by quantitative reverse transcription PCR. The results were considered significant when the *p*-value was less than 0.05.

3. Result

3.1. Effects of CTD on the cell number of SH-SY5Y cells

To determine the potential effects of CTD on human neuroblastoma SH-SY5Y cells, the cell growth assays were conducted. As shown in Fig. 1A, CTD dose-dependently stimulated the cell growth and one-way ANOVA showed that there were significant differences at Day 1 [$F(2, 12) = 11.150$, $p < 0.01$] and Day 2 [$F(2, 12) = 5.764$, $p < 0.05$]. The high concentration of CTD (100 μM) significantly increased the relative cell number at Day 1 ($p < 0.01$) and Day 2 ($p < 0.05$). Low concentrations of CTD (1 μM) also increased the relative cell number at Day 1 ($p < 0.05$), but not significantly at Day 2. The dose-response relationship between the exposure concentration and the growth stimulating effect of CTD was evaluated by the

WST-8 assay. The dose-response curves showed that CTD had growth stimulating effects on SH-SY5Y cells with an EC50 of 577 nM (Fig. 1B).

3.2. Antagonists to nAChR blocked the growth stimulating effect of CTD on SH-SY5Y cells

We therefore investigated whether the effects of CTD on the SH-SY5Y cells were mediated by human-type nAChRs. Although 10 μM mecamylamine (MEC), a broad spectrum non-competitive nAChRs antagonist, had no effect on the SH-SY5Y cells alone, it inhibited the growth stimulating effect of 100 μM CTD (Fig. 2A). Two-way ANOVA showed that there was no effect of MEC [$F(1, 16) = 3.295$] and significant effect of CTD [$F(1, 16) = 7.853$, $p < 0.05$] and significant interaction [$F(1, 16) = 12.887$, $p < 0.01$]. According to a previous report showing that SH-SY5Y cells are known to express α3, α7, β2 and β4 subunit of nAChRs (Groot Kormelink and Luyten, 1997), we further examined which subunit of nAChRs is involved in the effects of CTD with using subunit specific competitive nAChR antagonists. As shown in Fig. 2B and 2C, the α7 and β2 subunit specific antagonists methyllycaconitine (MLA, 100 nM) and dihydro-β-erythroidine (DHβE, 10 μM) did not suppress the effects of CTD. There was no effect of antagonists [MLA: $F(1, 16) = 1.964$; DHβE: $F(1, 16) = 4.191$], and significant effects of CTD were observed [MLA: $F(1, 16) = 15.817$, $p < 0.01$; DHβE: $F(1, 16) = 16.005$, $p < 0.01$]. No interaction was detected between CTD and antagonists [MLA: $F(1, 16) = 4.743$; DHβE: $F(1, 16) = 0.009$]. In contrast, an α3β4 specific antagonist, SR 16584 (10 μM), blocked the effect induced by 100 μM CTD (Fig. 2D). Two-way ANOVA showed that there was no effect of SR 16584 [$F(1, 16) = 2.602$] and significant effect of CTD [$F(1, 16) = 10.179$, $p < 0.05$] and significant interaction [$F(1, 16) = 8.312$, $p < 0.05$].

3.3. CTD evoked intracellular calcium flux in SH-SY5Y cells

As nAChRs are ligand-gated ion channels permeable to calcium ions, we next evaluate the CTD-induced changes of intracellular calcium levels in SH-SY5Y cells loaded with calcium-sensitive dye Fluo-4 AM. The temporal changes of intracellular calcium levels were monitored by fluorescence intensity of fluo-4 (F) normalized to the average of baseline intensity (F0). As shown in Fig. 3A, transient increases of fluorescence intensity were observed immediately after exposure to CTD. Quantitative analyses showed that both the maximum amplitude (Fmax-F0) [$F(3, 11) = 5.674$, $p < 0.05$] and the area under the curve [$F(3, 11) = 8.415$, $p < 0.01$] were significantly increased by at least 10 μM of CTD (Fig. 3B and 3C).

3.4. Effects of CTD on phosphorylation levels of ERK in SH-SY5Y cells

To examine the modulation of the intracellular signaling subsequent to intracellular calcium influx induced by CTD, we analyzed phosphorylation levels of extracellular signal-regulated kinase 1/2 (ERK), which is known to be important in proliferation of neuroblastoma cells (Stafman and Beierle, 2016). SH-SY5Y cells were exposed to CTD for 1 h, and total and phosphorylated ERK were detected on the same membrane at once by western blotting. As shown in Fig. 4A, although the band intensity of total ERK did not change, CTD increased that of phosphorylated ERK (p-ERK) compared to the control samples. Quantitative analyses showed that CTD dose-dependently and significantly increased the p-ERK/ERK ratio [$F(3, 11) = 4.053$, $p < 0.05$] (Fig. 4B).

3.5. Effects of CTD on global gene expression of SH-SY5Y cells

To understand changes of gene expression involved in the mechanisms of effects of CTD,

the transcriptome analysis was performed in cells exposed to 1 μM CTD for 24 h using GeneChip system and the clariom S human array with 21,448 probe sets. After normalization of obtained intensities of probes using the RMA algorithm using the GeneSpring software, low intensity probes (<10% expression level) were cutoff as noise. We then identified differentially expressed genes (174 up-regulated and 151 down-regulated) with at least 1.5-fold change compared with the control group (0.1% DMSO), and then conducted bioinformatical analyses to reveal biological functions, canonical pathways, and networks of differentially expressed genes based on Ingenuity Pathway Analysis (IPA) knowledge base software. We obtained little findings related to the phenotypic changes observed in this study from up-regulated genes (Supplemental Materials). The top 25 biological functions with positive z-scores related to the down-regulated genes are summarized in Table 2. Notably, CTD significantly decreased the expression of genes associated with neural functions with annotations of "Formation of filopodia," "Brain lesion," "Quantity of neurons," "Behavior," and "Differentiation of nervous system." Additionally, multiple annotations associated with calcium signaling, "Flux of Ca^{2+}," "Influx of Ca^{2+}," and "Ion homeostasis of cells," were also listed. The differentially activated or suppressed canonical pathways in down-regulated genes are shown in Fig. 5A. Canonical pathways including "Axonal Guidance Signaling" and "Synaptic Long Term Depression" relating to neural function were enriched in down-regulated genes. Cytoskeletal pathways, "Gα12/13 Signaling," "PAK Signaling," "Actin Cytoskeleton Signaling," and "Signaling by Rho Family GTPases," were significantly suppressed. Network analyses revealed gene networks with 40 molecules involved in "Cardiovascular System Development and Function," "Organismal Development" and "Cell-To-Cell Signaling and Interaction" (Fig. 5B) and several down-regulated genes indirectly affected signal transduction molecules such as ERK, ras-related protein 1 (Rap1)

and cAMP response element binding protein (Creb).

3.6. Validation of microarray results by quantitative reverse transcription PCR

To confirm the microarray results, the expression levels of down-regulated genes were measured by quantitative reverse transcription PCR. We chose three genes significant in the bioinformatical analyses by the IPA software including neuronal differentiation 4 (NEUROD4), adrenoceptor beta 2 (ADRB2), and neurotensin (NTS). As shown in Fig. 6, quantitative results showed that 1 μM of CTD significantly suppressed the expression of these genes ($p < 0.05$), which were the same pattern in microarray results.

3.7. Effects of CTD on neurite outgrowth of SH-SY5Y cells

In order to examine the neurodifferentiative effects of micromolar concentrations of CTD, we treated differentiating cells with CTD and morphologically evaluated the neurite outgrowth. As shown in Fig. 7A, neurites in differentiated cells were visualized by immunofluorescent staining with the neurite marker MAP2 (microtubule-associated protein 2). Quantitative analyses revealed that at least 1 μM of CTD significantly increased neurite length compared to the control group (Fig. 7B) [$F(3, 13) = 12.711$, $p < 0.01$]. The number of neurites per cell was not significantly changed by CTD (Fig. 7C) [$F(3, 13) = 3.345$].

4. Discussion

In the present study, we investigated whether CTD affected human neuroblastoma SH-SY5Y cells to obtain information about the risks of neonicotinoids in the human nervous system. Unexpectedly, CTD dose-dependently increased the number of cells and nAChR antagonists inhibited the growth stimulating effect of CTD. We clarified some of the

underlying mechanisms of the effects of CTD mediating intracellular calcium flux, phosphorylation of signal transduction molecules and alteration of global gene expression. Although cytotoxic effects of millimolar concentrations of neonicotinoids on SH-SY5Y cells were previously reported (Skandrani et al., 2006; Şenyildiz et al., 2018), these results firstly demonstrated that micromolar concentrations have functional effects on human-derived neuronal cells, in part by changing the intracellular signaling. Taken together, our data would provide a new perspective into understanding the effects of non-lethal doses of neonicotinoids on human nervous systems.

One of the interesting findings of this study is the growth stimulating effects of CTD, consistent with previous work evaluating the effects of nicotine in the same cell line (Serres and Carney, 2006). At the cellular level, cholinergic signaling by exogenous stimulation regulates cellular activities such as apoptosis, cell survival, proliferation and differentiation (Resende and Adhikari, 2009). Excessive amounts of nicotinic agonists are lethal, but sublethal doses consistently had proliferative effects in nAChR-expressing cell lines such as HT29 colon cancer cells and A549 lung cancer cells (Wong et al., 2007; Mucchietto et al., 2018). Additionally, activation of nAChRs has neuroprotective effects in SH-SY5Y cells; for example, nAChRs activation alleviated neurotoxicity of okadaic acid and amyloid-β (Del Barrio et al., 2011; Xue et al., 2015). Although the proliferation of neural cells was observed in limited areas in the mature brain, an *in vivo* study showed that an α7 nicotinic agonist reactivated adult neurogenesis in cortex and hippocampus in mice (Narla et al., 2013). Taken together, further studies should be carried out focusing on the effects of neonicotinoids on proliferative and differentiative neural stem cells in developing brains.

Our results showed that concomitant exposure to nAChR antagonists inhibited the growth stimulating effects of CTD. Given that these antagonists are active against human nAChRs,

our findings raise the likelihood that human-type nAChRs could be affected by neonicotinoids. Neuronal nAChRs are composed of pentamer structure and largely divided into four groups by subunit composition: (i) α7 homomers, (ii) α4 and β2 heteromers, (iii) α3, β4 and β2 heteromers and (iv) α2, α4 and β4 heteromers (Albuquerque et al., 2009). To date, previous studies have reported that CTD modulates electrophysiological responses to acetylcholine in human embryonic kidney (HEK293) cells expressing human α4β2 nAChRs, and in Xenopus oocytes expressing rat α7 nAChRs (Li et al., 2011; Cartereau et al., 2018). In this study, we used human neuroblastoma SH-SY5Y cells expressing α3, α7, β2, and β4 subunits (Groot Kormelink and Luyten, 1997). Our results showed that mecamylamine and SR 16584 inhibited the increasing of the cell number, indicating that α3β4 nAChRs are largely responsible for the effects of CTD. As described above, α3β4 nAChRs are frequently called “ganglion type” nAChRs, but they also play important roles in broad regions of mammal brain including hippocampus, medial habenula, pineal gland, cerebellum, locus coeruleus, substantia nigra and ventral tegmental area (Gotti, et al., 2006). Compared to other types of nAChRs, the current responses of α3β4 nAChRs to nicotinic agonists are slow but strong and durable (Chavez-Noriega et al., 1997), which may lead to the functional effects and phenotypic changes observed in this study. A recent study also revealed that the neonicotinoid IMI facilitates the expression of tyrosine hydroxylase, a marker of differentiation in PC12D cells mediated by rat α3β4 and α7 nAChRs (Kawahata and Yamakuni, 2018); thus, human α3β4 nAChRs could be significant to understanding the unexpected effects of neonicotinoids.

Neuronal nAChRs function as non-selective cation channels permeable to calcium ions. Cation influx by nAChRs subsequently raises the intracellular calcium concentration by activating voltage-dependent calcium channels (VDCCs) with membrane depolarization and

calcium release by ryanodine receptors from endoplasmic reticulum (Shen and Yakel, 2009). In this study, micromolar concentrations of CTD dose-dependently evoked the transient increase of intracellular calcium level for a few tens of seconds. These temporal patterns are very similar to intracellular calcium responses to micromolar concentrations of nicotine; such responses are partly mediated by α7 nAChRs and depend to a large part on VDCCs (Dajas-Bailador et al., 2002a; Gilbert et al., 2009). Transcriptome analysis by Kimura-Kuroda et al., (2016) showed that 1 μM nicotine and two neonicotinoids (ACE and IMI) commonly altered the gene expression of VDCC subunits in rat cerebellar cells. Another *in vivo* study consistently demonstrated that CTD-induced dopamine release in rat striatum is related to neuronal membrane depolarization (Faro et al., 2012). Our result also showed that gene sets related "Flux of Ca^{2+}," "Influx of Ca^{2+}," and "Ion homeostasis of cells" were significantly enriched in the CTD-down-regulated genes, which may be a result of negative feedback by sustained higher intracellular calcium with membrane depolarization.

Mitogen-activated protein kinases play crucial roles in neural cells for transmitting exogenous stimulation to intracellular signaling. In particular, ERK regulates cell proliferation, differentiation, survival, and migration. In this study, we found that CTD dose-dependently increased the phosphorylation level of ERK, consistent with other studies in mouse neuroblastoma N1E-115 cells (Tomizawa and Casida, 2002) and SH-SY5Y cells (Dajas-Bailador et al., 2002b). These studies consistently demonstrated that phosphorylation states of ERK were altered by nAChR-mediated calcium signaling and membrane depolarization. In rat PC12h cells, ERK phosphorylation by nicotinic ligands is inhibited by α3β4 nAChRs (Nakayama et al., 2006) and over-expression of α7 nAChRs promotes the basal level of p-ERK (Utsugisawa et al., 2002). Our network analyses showed that most of the down-regulated genes indirectly act upstream of ERK, which may support the modulation

of ERK activation induced by CTD. It also should be noted that neonicotinoids, including CTD are immediately metabolized inside the body of mammals, and certain amounts of metabolites of neonicotinoids are detected in the brain (Fold and Casida, 2006). Other studies demonstrated that metabolites of IMI had higher affinity for human nAChRs and induced strong activation of ERK than that of the original compound (Tomizawa and Casida 2002, 2005), indicating that additional studies should be conducted focusing on the potential effects of metabolites of neonicotinoids. Considering that ERK signaling controls neuroplasticity and synaptic transmission in the brain (Thomas and Huganir, 2004), we should consider the risks of neonicotinoids on higher brain function such as learning and memory.

Microarray analyses revealed different aspects of the effects of CTD, indicating that 24 h exposure of 1 μM CTD could disrupt several sets of gene expression involved in cytoskeleton regulatory signaling. A series of studies recently showed that α7 nAChRs coupled to G-proteins and regulated cytoskeletal dynamics and axon growth (King et al., 2015; Kabbani and Nichols, 2018), suggesting intracellular calcium flux mediated by nAChRs also associated with morphological changes of neuronal cells. In this study, our data indicated that down-regulated genes contained significantly enriched biological functions of "Formation of filopodia," essential for advancing growth cones to extend neurites at the tip of the axon. It was also noted that "Axon guidance signaling" was the most significantly enriched pathway with no activity pattern available and "Differentiation of nervous system" was the significantly enriched biological function in the down-regulated genes by CTD. Therefore, we investigated whether CTD had an impact on neurite outgrowth in differentiating SH-SY5Y cells. We observed increased length and number of neurite in differentiated SH-SY5Y cells by CTD exposure, both of which disagree with previous studies reporting that ACE and IMI suppressed neurite outgrowth in rat Purkinje cells (Kimura-Kuroda et al., 2016).

Furthermore, another study reported that four neonicotinoids had no effect on neurite length of PC12 cells (Christen et al., 2017). Nordman and Kabbani (2012) showed that nicotinic agonists inhibited neurite surface area in PC12 cells, whereas a nicotinic antagonist for α7 nAChRs, α-bungarotoxin promoted it. These inconsistencies among studies may reflect differences in species, cell type, and receptor properties.

In conclusion, the present study demonstrated for the first time that CTD had functional effects on human neuroblastoma SH-SY5Y cells that resulted in increased cell growth mediated by human nAChRs. Moreover, our data showed that micromolar concentrations of CTD acutely disrupted intracellular signaling that led to an influx of intracellular calcium, phosphorylation of ERK and alteration of global gene expression. Transcriptional and neuromorphological changes strongly suggest that CTD has impacts on neuronal differentiation and neurite outgrowth. Taken together, our data provide novel toxicological information to assess the risk of neonicotinoids on human health by using a human-derived cell line with neuronal properties. Additional research is needed to understand the risk of environmentally-relevant doses of neonicotinoids, with a focus on developmental events in the brain such as neural differentiation, migration, and neural circuit development.

Conflict of interest

The authors declare that they have no conflict of interest.

Funding

This work was supported by a Grant-in-Aid for Research Activity Start-up (JSPS KAKENHI Grant Number JP17H06706) and a Grant-in-Aid for Early-Career Scientists (JP19K19406) to T Hirano.

Acknowledgments

The authors thank all members of the life science research center for their technical assistance.

References

Albuquerque, E. X., Pereira, E. F., Alkondon, M., Rogers, S. W., 2009. Mammalian nicotinic acetylcholine receptors: from structure to function. Physiol. Rev. 89, 73–120.

Anderson, D. J., Bunnelle, W., Surber, B., Du, J., Surowy, C., Tribollet, E., Marguerat, A., Bertrand, D., Gopalakrishnan, M., 2008. [^{3}H]A-585539 [(1S,4S)-2,2-dimethyl-5-(6-phenylpyridazin-3-yl)-5-aza-2-azoniabicyclo[2.2.1]heptane], a novel high-affinity α7 neuronal nicotinic receptor agonist: radioligand binding characterization to rat and human brain. J. Pharmacol. Exp. Ther. 324, 179–187.

Burke, A. P., Niibori, Y., Terayama, H., Ito, M., Pidgeon, C., Arsenault, J., Camarero, P. R., Cummins, C. L., Mateo, R., Sakabe, K., Hampson, D. R., 2018. Mammalian susceptibility to a neonicotinoid insecticide after fetal and early postnatal exposure. Sci. Rep. 8, 16639.

Cartereau, A., Martin, C., Thany, S. H., 2018. Neonicotinoid insecticides differently modulate acetycholine-induced currents on mammalian α7 nicotinic acetylcholine receptors. Br. J. Pharmacol. 175, 1987–1998.

Casida, J. E., 2018. Neonicotinoids and other insect nicotinic receptor competitive modulators: progress and prospects. Annu. Rev. Entomol. 63, 125–144.

Chavez-Noriega, L. E., Crona, J. H., Washburn, M. S., Urrutia, A., Elliott, K. J., Johnson, E. C., 1997. Pharmacological characterization of recombinant human neuronal nicotinic acetylcholine receptors hα2β2, hα2β4, hα3β2, hα3β4, hα4β2, hα4β4 and hα7 expressed in *Xenopus* oocytes. J. Pharmacol. Exp. Ther. 280, 346–356.

Chen, M., Tao, L., McLean, J., Lu, C., 2014. Quantitative analysis of neonicotinoid insecticide residues in foods: implication for dietary exposures. J. Agric. Food Chem. 62, 6082–6090.

Christen, V., Rusconi, M., Crettaz, P., Fent, K., 2017. Developmental neurotoxicity of different pesticides in PC-12 cells *in vitro*. Toxicol. Appl. Pharmacol. 325, 25–36.

Cimino, A. M., Boyles, A. L., Thayer, K. A., Perry, M. J., 2017. Effects of neonicotinoid pesticide exposure on human health: A systematic review. Environ. Health Perspect. 125, 155–162.

Dajas-Bailador, F. A., Mogg, A. J., Wonnacott, S., 2002a. Intracellular Ca^{2+} signals evoked by stimulation of nicotinic acetylcholine receptors in SH-SY5Y cells: contribution of voltage-operated Ca^{2+} channels and Ca^{2+} stores. J. Neurochem. 81, 606–614.

Dajas-Bailador, F. A., Soliakov, L., Wonnacott, S., 2002b. Nicotine activates the extracellular signal-regulated kinase 1/2 via the α7 nicotinic acetylcholine receptor and protein kinase A, in SH-SY5Y cells and hippocampal neurones. J. Neurochem. 80, 520–530.

Dani, J. A., Bertrand, D., 2007. Nicotinic acetylcholine receptors and nicotinic cholinergic mechanisms of the central nervous system. Annu. Rev. Pharmacol. Toxicol. 47, 699–729.

Del Barrio, L., Martín-de-Saavedra, M. D., Romero, A., Parada, E., Egea, J., Avila, J., McIntosh, J. M., Wonnacott, S., López, M. G., 2011. Neurotoxicity induced by okadaic acid in the human neuroblastoma SH-SY5Y line can be differentially prevented by α7 and β2 nicotinic stimulation. Toxicol. Sci. 123, 193–205.

Faro, L. R., Oliveira, I. M., Durán, R., Alfonso, M., 2012. In vivo neurochemical characterization of clothianidin induced striatal dopamine release. Toxicology 302, 197–202.

Ford, K. A., Casida, J. E., 2006. Unique and common metabolites of thiamethoxam, clothianidin, and dinotefuran in mice. Chem. Res. Toxicol. 19, 1549–1556.

Gibbons, D., Morrissey, C., Mineau, P., 2015. A review of the direct and indirect effects of neonicotinoids and fipronil on vertebrate wildlife. Environ. Sci. Pollut. Res. Int. 22, 103–118.

Gilbert, D., Lecchi, M., Arnaudeau, S., Bertrand, D., Demaurex, N., 2009. Local and global calcium signals associated with the opening of neuronal α7 nicotinic acetylcholine receptors. Cell Calcium 45, 198–207.

Gotti, C., Zoli, M., Clementi, F., 2006. Brain nicotinic acetylcholine receptors: native subtypes and their relevance. Trends Pharmacol. Sci. 27, 482–491.

Groot Kormelink, P. J., Luyten, W. H., 1997. Cloning and sequence of full-length cDNAs encoding the human neuronal nicotinic acetylcholine receptor (nAChR) subunits β3 and β4 and expression of seven nAChR subunits in the human neuroblastoma cell line SH-SY5Y and/or IMR-32. FEBS Lett. 400, 309–314.

Hirano, T., Yanai, S., Omotehara, T., Hashimoto, R., Umemura, Y., Kubota, N., Minami, K., Nagahara, D., Matsuo, E., Aihara, Y., Shinohara, R., Furuyashiki, T., Mantani. Y., Yokoyama, T., Kitagawa, H., Hoshi, N., 2015. The combined effect of clothianidin and environmental stress on the behavioral and reproductive function in male mice. J. Vet. Med. Sci. 77, 1207–1215.

Hirano, T., Yanai, S., Takada, T., Yoneda, N., Omotehara, T., Kubota, N., Minami, K., Yamamoto, A., Mantani, Y., Yokoyama, T., Kitagawa, H., Hoshi, N., 2018. NOAEL-dose of a neonicotinoid pesticide, clothianidin, acutely induce anxiety-related behavior with human-audible vocalizations in male mice in a novel environment. Toxicol. Lett. 282, 57–63.

Hoshi, N., Hirano, T., Omotehara, T., Tokumoto, J., Umemura,Y., Mantani, Y., Tanida, T., Warita, K., Tabuchi, Y., Yokoyama, T., Kitagawa, H., 2014. Insight into the mechanism of reproductive dysfunction caused by neonicotinoid pesticides. Biol. Pharm. Bull. 37, 1439–1443.

Ikenaka, Y., Fujioka, K., Kawakami, T., Ichise, T., Bortey-Sam, N., Nakayama, S. M. M., Mizukawa, H., Taira, K., Takahashi, K., Kato, K., Arizono, K., Ishizuka, M., 2018. Contamination by neonicotinoid insecticides and their metabolites in Sri Lankan black tea leaves and Japanese green tea leaves. Toxicol. Rep. 5, 744–749.

Ikenaka, Y., Miyabara, Y., Ichise, T., Nakayama, S., Nimako, C., Ishizuka, M., Tohyama, C., 2019. Exposures of children to neonicotinoids in pine wilt disease control areas. Environ. Toxicol. Chem. 38, 71–79.

Kabbani, N., Nichols, R. A., 2018. Beyond the channel: metabotropic signaling by nicotinic receptors. Trends Pharmacol. Sci. 39, 354–366.

Kawahata, I., Yamakuni, T., 2018. Imidacloprid, a neonicotinoid insecticide, facilitates tyrosine hydroxylase transcription and phenylethanolamine *N*-methyltransferase mRNA expression to enhance catecholamine synthesis and its nicotine-evoked elevation in PC12D cells. Toxicology 394, 84–92.

Kimura-Kuroda, J., Komuta, Y., Kuroda, Y., Hayashi, M., Kawano, H., 2012. Nicotine-like effects of the neonicotinoid insecticides acetamiprid and imidacloprid on cerebellar neurons from neonatal rats. PLoS One 7, e32432.

Kimura-Kuroda, J., Nishito, Y., Yanagisawa, H., Kuroda, Y., Komuta, Y., Kawano, H., Hayashi, M., 2016. Neonicotinoid insecticides alter the gene expression profile of neuron-enriched cultures from neonatal rat cerebellum. Int. J. Environ. Res. Public Health 13, 987.

King, J. R., Nordman, J. C., Bridges, S. P., Lin, M. K., Kabbani, N., 2015. Identification and

characterization of a G protein-binding cluster in α7 nicotinic acetylcholine receptors. J. Biol. Chem. 290, 20060–20070.

Kovalevich, J., Langford, D., 2013. Considerations for the use of SH-SY5Y neuroblastoma cells in neurobiology. Methods Mol. Biol. 1078, 9–21.

Li, P., Ann, J., Akk, G., 2011. Activation and modulation of human α4β2 nicotinic acetylcholine receptors by the neonicotinoids clothianidin and imidacloprid. J. Neurosci. Res. 89, 1295–1301.

Lukas, R. J., Norman, S. A., Lucero, L., 1993. Characterization of nicotinic acetylcholine receptors expressed by cells of the SH-SY5Y human neuroblastoma clonal line. Mol. Cell. Neurosci. 4, 1–12.

Mucchietto, V., Fasoli, F., Pucci, S., Moretti, M., Benfante, R., Maroli, A., Di Lascio, S., Bolchi, C., Pallavicini, M., Dowell, C., McIntosh, M., Clementi, F., Gotti, C., 2018. α9- and α7-containing receptors mediate the pro-proliferative effects of nicotine in the A549 adenocarcinoma cell line. Br. J. Pharmacol. 175, 1957–1972.

Nakayama, H., Shimoke, K., Isosaki, M., Satoh, H., Yoshizumi, M., Ikeuchi, T., 2006. Subtypes of neuronal nicotinic acetylcholine receptors involved in nicotine-induced phosphorylation of extracellular signal-regulated protein kinase in PC12h cells. Neurosci. Lett. 392, 101–104.

Narla, S., Klejbor, I., Birkaya, B., Lee, Y. W., Morys, J., Stachowiak, E. K., Terranova, C., Bencherif, M., Stachowiak, M. K., 2013. α7 nicotinic receptor agonist reactivates neurogenesis in adult brain. Biochem. Pharmacol. 86, 1099–1104.

Nordman, J. C., Kabbani, N., 2012. An interaction between α7 nicotinic receptors and a G-protein pathway complex regulates neurite growth in neural cells. J. Cell Sci. 125, 5502–5513.

Osaka, A., Ueyama, J., Kondo, T., Nomura, H., Sugiura, Y., Saito, I., Nakane, K., Takaishi, A., Ogi, H., Wakusawa, S., Ito, Y., Kamijima, M., 2016. Exposure characterization of three major insecticide lines in urine of young children in Japan— neonicotinoids, organophosphates, and pyrethroids. Environ. Res. 147, 89–96.

Papke, R. L., Porter Papke, J. K., 2002. Comparative pharmacology of rat and human α7 nAChR conducted with net charge analysis. Br. J. Pharmacol. 137, 49–61.

Resende, R. R, Adhikari, A., 2009. Cholinergic receptor pathways involved in apoptosis, cell proliferation and neuronal differentiation. Cell Commun. Signal. 7, 20.

Sano, K., Isobe, T., Yang, J., Win-Shwe, T. T., Yoshikane, M., Nakayama, S. F., Kawashima, T., Suzuki, G., Hashimoto, S., Nohara, K., Tohyama, C., Maekawa, F., 2016. *In utero* and lactational exposure to acetamiprid induces abnormalities in socio-sexual and anxiety-related behaviors of male mice. Front. Neurosci. 10, 228.

Şenyildiz, M., Kilinc, A., Ozden, S., 2018. Investigation of the genotoxic and cytotoxic effects of widely used neonicotinoid insecticides in HepG2 and SH-SY5Y cells. Toxicol. Ind. Health 34, 375–383.

Serres, F., Carney, S. L., 2006. Nicotine regulates SH-SY5Y neuroblastoma cell proliferation through the release of brain-derived neurotrophic factor. Brain Res. 1101, 36–42.

Sheets, L. P., Li, A. A., Minnema, D. J., Collier, R. H., Creek, M. R., Peffer, R. C., 2016. A critical review of neonicotinoid insecticides for developmental neurotoxicity. Crit. Rev. Toxicol. 46, 153–190.

Shen, J. X., Yakel, J. L., 2009. Nicotinic acetylcholine receptor-mediated calcium signaling in the nervous system. Acta Pharmacol. Sin. 30, 673–680.

Skandrani, D., Gaubin, Y., Beau, B., Murat, J. C., Vincent, C., Croute, F., 2006. Effect of

selected insecticides on growth rate and stress protein expression in cultured human A549 and SH-SY5Y cells. Toxicol. In Vitro 20, 1378–1386.

Stafman, L. L., Beierle, E. A., 2016. Cell proliferation in neuroblastoma. Cancers (Basel) 8, 13.

Stokes, C., Treinin, M., Papke, R. L., 2015. Looking below the surface of nicotinic acetylcholine receptors. Trends Pharmacol. Sci. 36, 514–523.

Takada, T., Yoneda, N., Hirano, T., Yanai, S., Yamamoto, A., Mantani, Y., Yokoyama, T., Kitagawa, H., Tabuchi, Y., Hoshi, N., 2018. Verification of the causal relationship between subchronic exposures to dinotefuran and depression-related phenotype in juvenile mice. J. Vet. Med. Sci. 80, 720–724.

Thomas, G. M., Huganir, R. L., 2004. MAPK cascade signalling and synaptic plasticity. Nat. Rev. Neurosci. 5, 173–183.

Tomizawa, M., Casida, J. E., 2002. Desnitro-imidacloprid activates the extracellular signal-regulated kinase cascade via the nicotinic receptor and intracellular calcium mobilization in N1E-115 cells. Toxicol. Appl. Pharmacol. 184, 180–186.

Tomizawa, M., Casida, J. E., 2005. Neonicotinoid insecticide toxicology: mechanisms of selective action. Annu. Rev. Pharmacol. Toxicol. 45, 247–268.

Tsunoyama, K., Gojobori, T., 1998. Evolution of nicotinic acetylcholine receptor subunits. Mol. Biol. Evol. 15, 518–527.

Ueyama, J., Harada, K. H., Koizumi, A., Sugiura, Y., Kondo, T., Saito, I., Kamijima, M., 2015. Temporal levels of urinary neonicotinoid and dialkylphosphate concentrations in Japanese women between 1994 and 2011. Environ. Sci. Technol. 49, 14522–14528.

Utsugisawa, K., Nagane, Y., Obara, D., Tohgi, H., 2002. Over-expression of α7 nicotinic acetylcholine receptor induces sustained ERK phosphorylation and N-cadherin expression in PC12 cells. Brain Res. Mol. Brain Res. 106, 88–93.

Wang, X., Anadón, A., Wu, Q., Qiao, F., Ares, I., Martínez-Larrañaga, M. R., Yuan, Z., Martínez, M. A., 2018. Mechanism of neonicotinoid toxicity: Impact on oxidative stress and metabolism. Annu. Rev. Pharmacol. Toxicol. 58, 471–507.

Wong, H. P., Yu, L., Lam, E. K., Tai, E. K., Wu, W. K., Cho, C. H., 2007. Nicotine promotes cell proliferation via α7-nicotinic acetylcholine receptor and catecholamine-synthesizing enzymes-mediated pathway in human colon adenocarcinoma HT-29 cells. Toxicol. Appl. Pharmacol. 221, 261–267.

Xue, M., Zhu, L., Zhang, J., Qiu, J., Du, G., Qiao, Z., Jin, G., Gao, F., Zhang, Q., 2015. Low dose nicotine attenuates Aβ neurotoxicity through activation early growth response gene 1 pathway. PLoS One 10, e0120267.

Yoneda, N., Takada, T., Hirano, T., Yanai, S., Yamamoto, A., Mantani, Y., Yokoyama, T., Kitagawa, H., Tabuchi, Y., Hoshi, N., 2018. Peripubertal exposure to the neonicotinoid pesticide dinotefuran affects dopaminergic neurons and causes hyperactivity in male mice. J. Vet. Med. Sci. 80, 634–637.

Figure legends

Fig. 1. Effects of clothianidin (CTD) on the cell growth of SH-SY5Y cells. (A) Cell growth curve for SH-SY5Y cells exposed to 1 or 100 μM CTD. Relative cell number is determined as fold change in cell number relative to the number of cells initially plated. (B) Dose-response curve for the increases of cell number at 24 h of CTD exposure evaluated by WST-8 assay. Responses are normalized to the maximum response induced by 10 μM CTD and fitted to the 4-parameter sigmoidal equation. All data points are represented by at least five independent experiments and values are shown by the mean ± SD, † $p < 0.05$ CTD 1 μM vs. control group, and $*p < 0.05$, $**p < 0.01$ CTD 100 μM vs. control group (one-way ANOVA followed by Dunnett's post-hoc test).

Fig. 2. Effects of nicotinic acetylcholine receptors antagonists, (A) 10 μM mecamylamine (MEC; broad spectrum antagonist), (B) 100 nM methyllycaconitine (MLA; α7 selective antagonist), (C) 10 μM dihydro-β-erythroidine (DHβE; β2 selective antagonist) and (D) 10 μM SR 16584 (α3β4 selective antagonist) on the growth stimulating effect of 100 μM CTD. All data are represented by at least five independent experiments and values are shown by the mean ± SD, $*p < 0.05$, $**p < 0.01$ vs. other groups (two-way ANOVA followed by Tukey's post-hoc test).

Fig. 3. Effects of CTD on intracellular calcium level of SH-SY5Y cells evaluated by fluo-4 assay. (A) Time course of changes in the fluorescence intensity of fluo-4 evoked by CTD. Fluorescence intensity at each time point was normalized to the average level of the baseline intensity. The summarized data, (B) Fmax-F0 and (C) area under curve were calculated to quantitate the effect of CTD. F: fluorescence intensity; F0: average level of baseline

fluorescence intensity; Fmax: maximal value of fluorescence intensity after treatment. All data are represented by at least three independent experiments and values are shown by the mean ± SD, *$p < 0.05$, **$p < 0.01$ vs. control group (one-way ANOVA followed by Dunnett's post-hoc test).

Fig. 4. Effects of CTD on phosphorylation levels of extracellular signal-regulated kinase 1/2 (ERK) on SH-SY5Y cells analyzed by western blotting. (A) Representative images of bands of phosphorylated ERK (p-ERK) and total ERK on the same membrane. (B) Phosphorylation levels of ERK after 1 h exposure of CTD were calculated by band intensities of p-ERK normalized by those of total ERK. All data are represented by at least three independent experiments and values are shown by the mean ± SD, *$p < 0.05$ vs. control group (one-way ANOVA followed by Dunnett's post-hoc test).

Fig. 5. Canonical pathways and a gene network of 151 down-regulated genes (>1.5-fold) altered by 24 h exposure of 1 μM CTD identified by ingenuity pathway analysis (IPA) software. (A) Signaling pathways significantly enriched by Fisher's exact test were summarized. Solid and dotted squares showed pathways related to neural and cytoskeletal function. (B) A gene network map illustrated interactions of down-regulated genes (green colored) and other molecules.

Fig. 6. Validation of microarray results using quantitative reverse transcription PCR. Gene expression levels of neuronal differentiation 4 (NEUROD4), adrenoceptor beta 2 (ADRB2), neurotensin (NTS) in the control (white bar) and of CTD-exposed group (1 μM, blue bar) were calculated relative to the housekeeping gene, glyceraldehyde-3-phosphate

dehydrogenase (GAPDH) by comparison to the control group. All data are represented by at least three independent experiments and values are shown by the mean ± SD, *$p < 0.05$ vs. control group (Welch's *t* test).

Fig. 7. Effects of CTD on neurite outgrowth in differentiating SH-SY5Y cells. Cells were induced to differentiate for 6 days with or without CTD exposure. (A)Representative images of immunofluorescent staining of a neurite maker, MAP2 (microtubule-associated protein 2: red) with DAPI cell nuclear staining (blue) in the control, CTD 1 μM, CTD 10 μM and CTD 100 μM group. The average of (B) neurite length and (C) number of neurites per cell were measured by the image analysis. Bar = 100 μm. All data are represented by at least three independent experiments and values are shown by the mean ± SD, *$p < 0.05$, **$p < 0.01$ vs. control group (one-way ANOVA followed by Dunnett's post-hoc test).

Table1. Primer sequences used in quantitative reverse transcription PCR

Gene Symbol	Gene ID	Direction	Primer sequence (5'-3')
NEUROD4	NM_021191.3	foword	gggagagctagtcaacacac
(neuronal differentiation 4)		reverse	ttgggacccctctcttagg
ADRB2	NM_000024.5	foword	ggattgtgtcaggccttacc
(adrenoceptor beta 2)		reverse	gatcaccaggggaacgtaga
NTS	NM_006183.5	foword	ccttcagtgtgcttctgac
(neurotensin)		reverse	gcagagtcatcttccaagag
GAPDH	NM_001256799.2	foword	ccaccaactgcttagcac
(glyceraldehyde-3-phosphate dehydrogenase)		reverse	catcacgccacagtttcc

Table 2. Top 25 of biological functions of 151 down-regulated genes

Functions Annotation	*p*-Value	Predicted Activation State	Activation z-score	Number of Molecules
Size of body	9.46E-05	Decreased	-4.088	18
Formation of filopodia	4.74E-03	Decreased	-2.219	5
Flux of Ca^{2+}	5.64E-03	Decreased	-2.192	7
Binding of leukocyte cell lines	4.57E-04	Decreased	-2.000	4
Hydrolysis of nucleotide	6.18E-03		-1.949	4
Influx of Ca^{2+}	1.17E-02		-1.932	5
Ion homeostasis of cells	5.18E-03		-1.890	11
Adhesion of blood cells	7.08E-03		-1.857	8
Adhesion of tumor cell lines	7.04E-03		-1.680	7
Adhesion of immune cells	1.51E-02		-1.598	7
Leukocyte migration	4.62E-03		-1.341	15
Permeability of vascular system	1.52E-04		-1.164	7
Angiogenesis of tumor	8.02E-03		-1.131	4
Binding of hematopoietic cell lines	5.26E-05		-1.109	5
Brain lesion	4.55E-03		-0.927	15
Atherosclerosis	4.39E-03		-0.878	10
Growth of vessel	7.45E-04		-0.796	6
Advanced malignant tumor	8.25E-03		-0.594	15
Quantity of neurons	1.16E-02		-0.527	8
Cancer of cells	1.29E-02		-0.384	46
Neoplasia of cells	4.51E-03		-0.350	49
Behavior	7.85E-03		-0.046	16
Lymphatic system tumor	8.34E-03		0.926	24
Differentiation of nervous system	1.42E-02		1.342	9
Organismal death	9.36E-03	Increased	4.755	30

activation z-score; >2.0 or < -2.0 is significantly predictive

699

Figure
Click here to download high resolution image

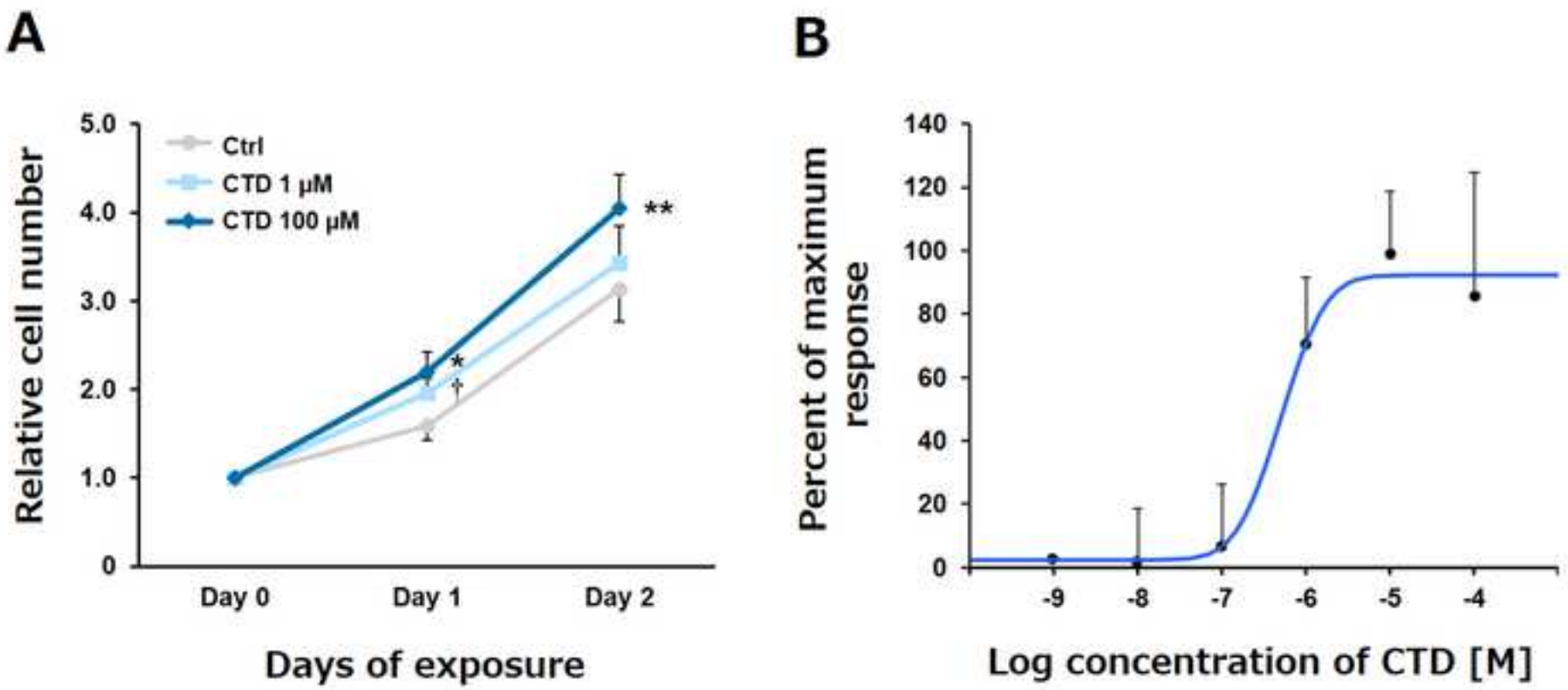

Figure

Click here to download high resolution image

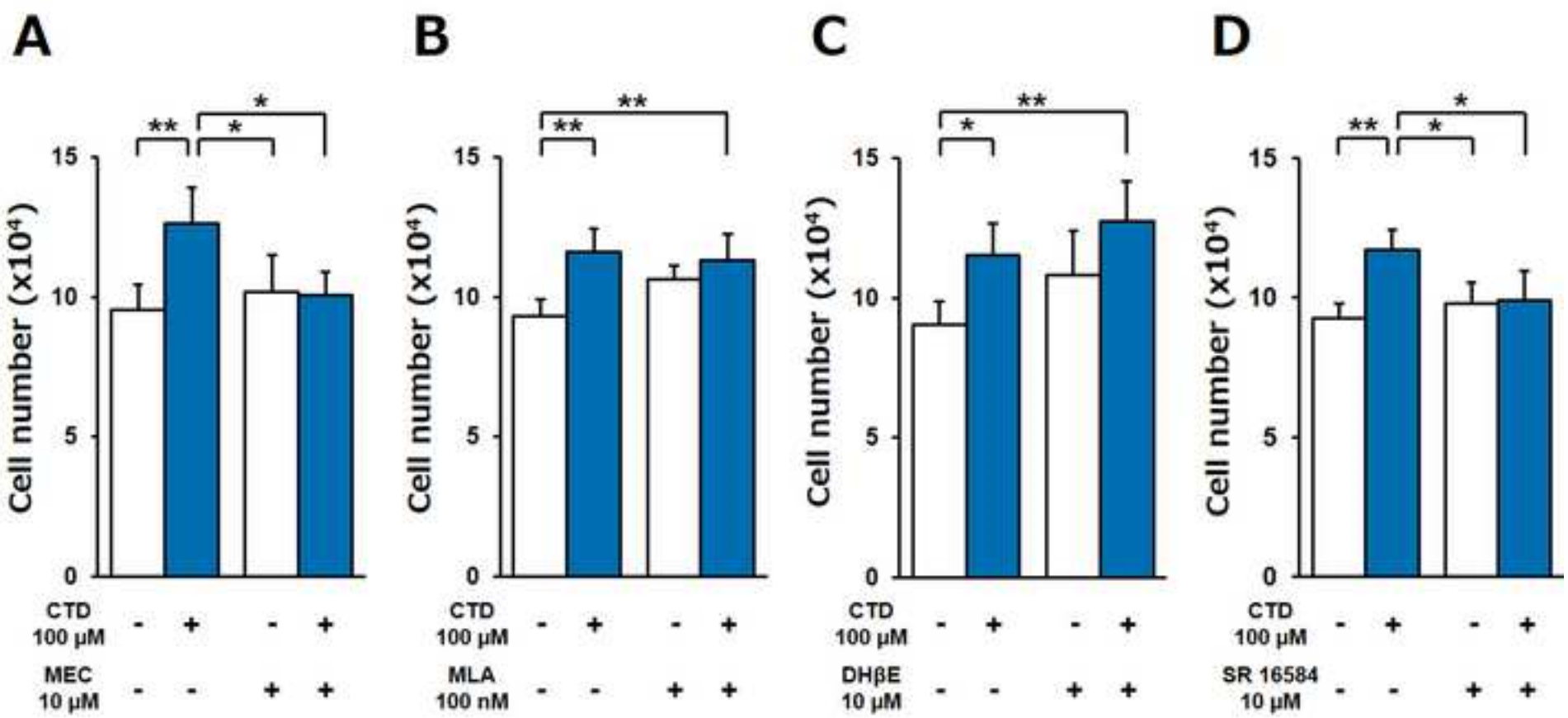

Figure
Click here to download high resolution image

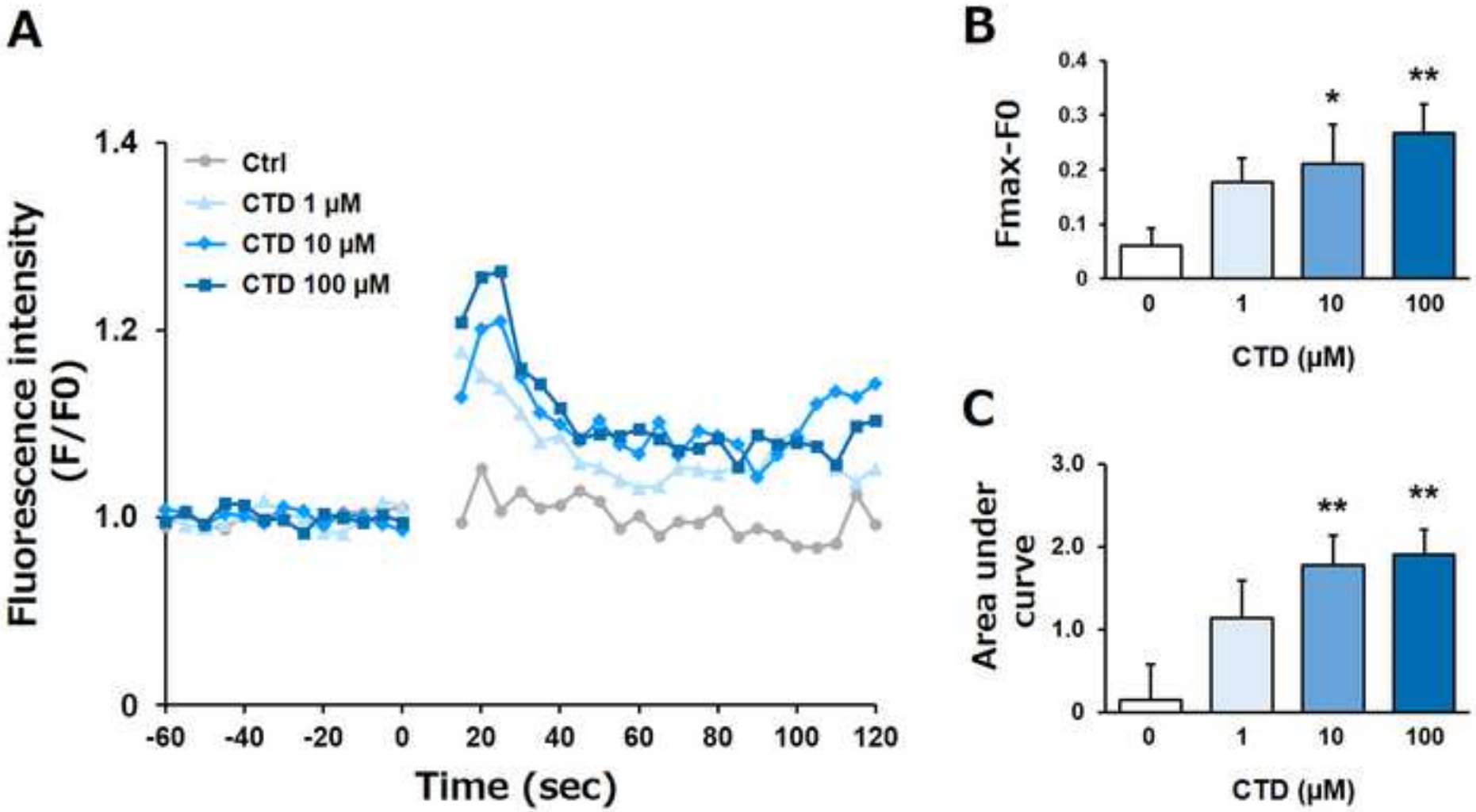

Figure
Click here to download high resolution image

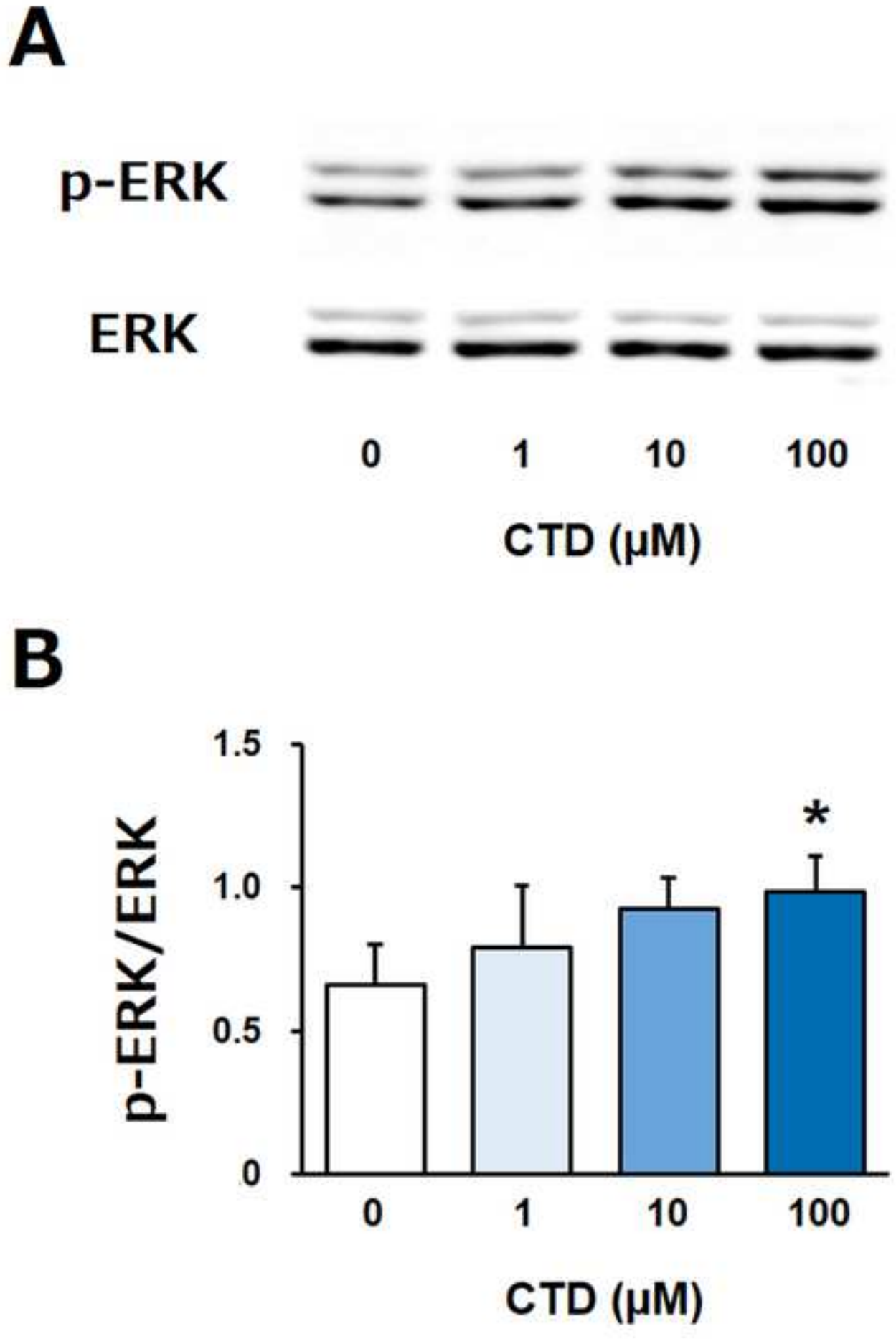

Figure
Click here to download high resolution image

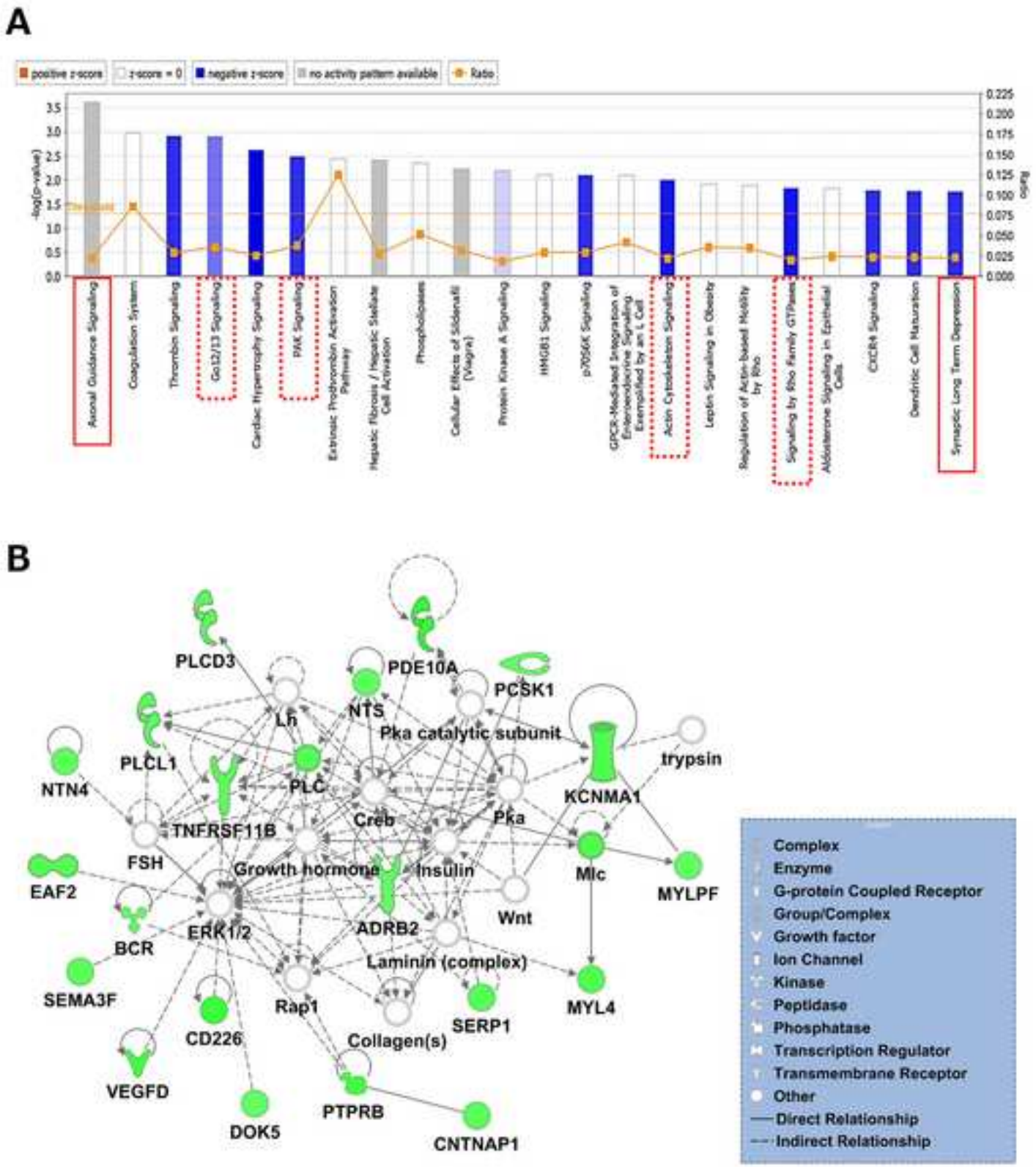

Figure
Click here to download high resolution image

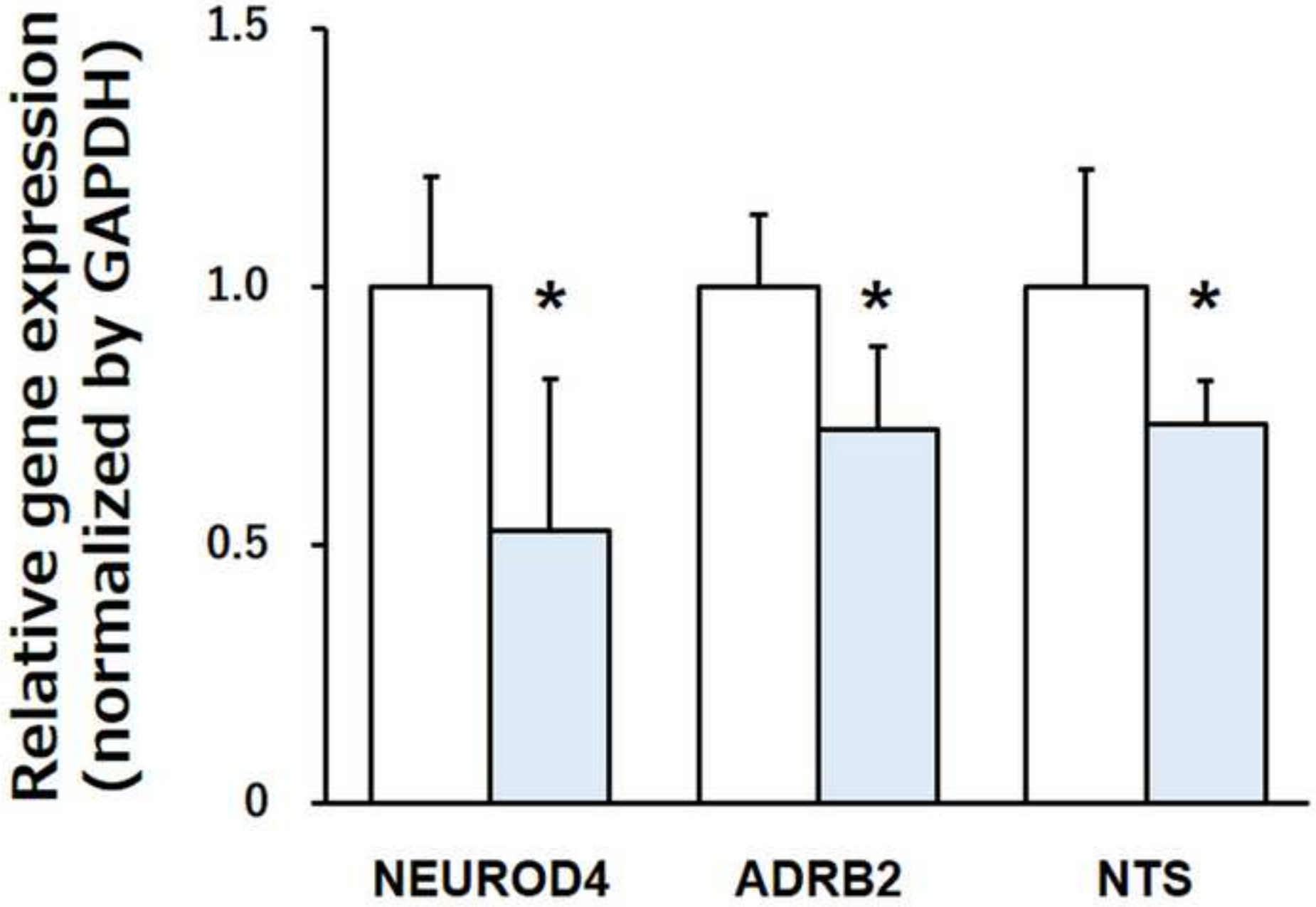

Figure
Click here to download high resolution image

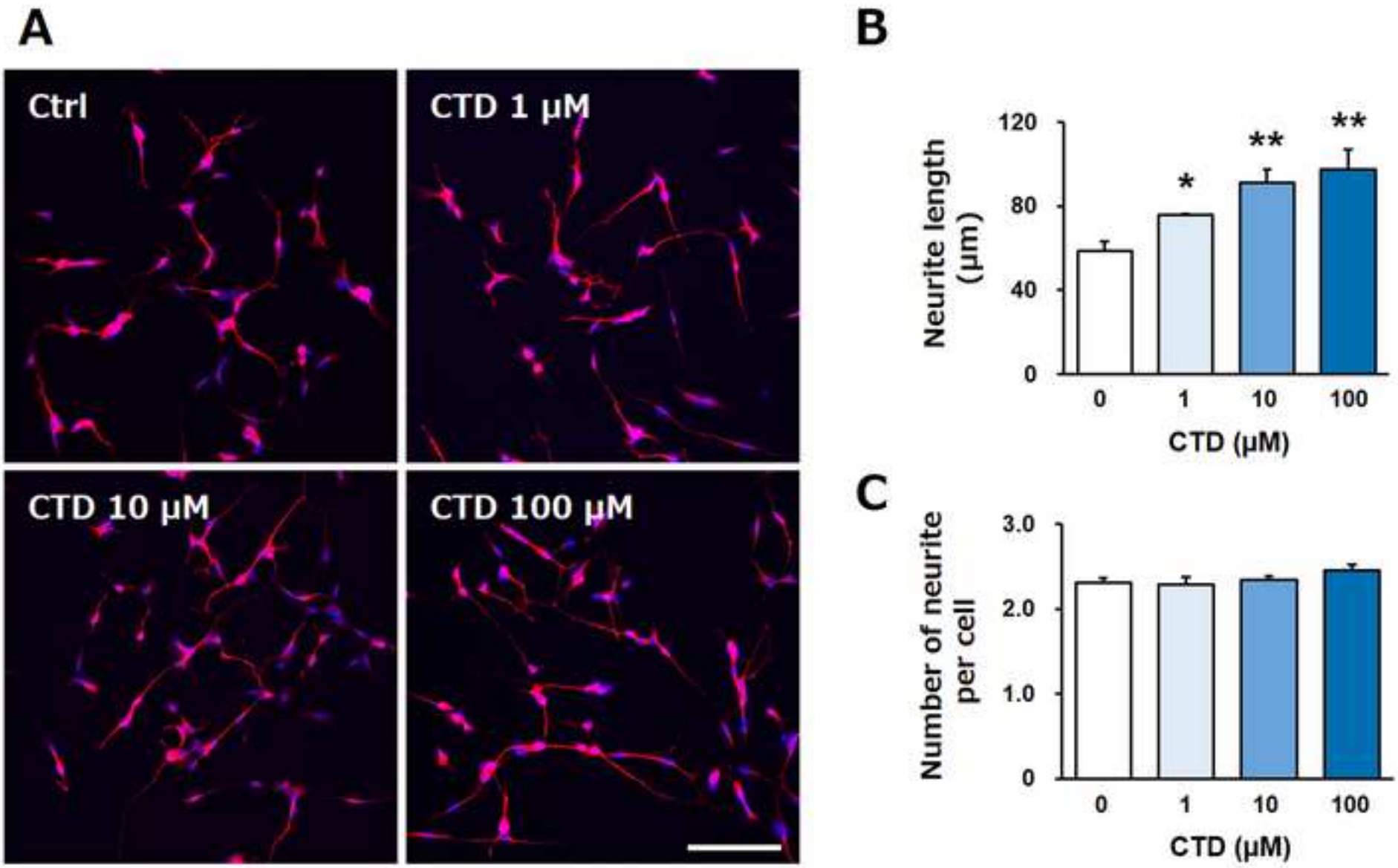

Supplementary Material

Click here to download Supplementary Material: Supplemental Materials _THirano.xlsx